

Light scattering from nonspherical airborne particles: experimental and theoretical comparisons

Edwin Hirst, Paul H. Kaye, and John R. Guppy

A laser light-scattering instrument has been designed to permit an investigation of the spatial intensity distribution of light scattered by individual airborne particles constrained within a laminar flow, with a view to providing a means of classifying the particles in terms of their shape and size. Ultimately, a means of detecting small concentrations of potentially hazardous particles, such as asbestos fiber, is sought. The instrument captures data relating to the spatial distribution of light scattered from individual particles in flow. As part of an investigation to optimize orientation control over particles within the sample airstream, the instrument has been challenged with nonspherical particles of defined shape and size, and a simple theoretical treatment based on the Rayleigh-Gans formalism has been used to model the spatial intensity distribution of light scattered from these particle types and hence derive particle orientation data. Both experimental and theoretical scattering data are presented, showing good agreement for all particle types examined.

Key words: Light scattering, nonspherical particles.

Introduction

In the fields of occupational hygiene and environmental monitoring, there is international recognition of the need for new techniques and instrumentation for the detection and monitoring of potentially hazardous respirable airborne particulates, especially in working environments.¹ Particle types of concern include asbestos and other mineral fibers resulting from building-clearance operations and airborne microorganisms (e.g., *Legionella pneumophila*) that may be generated within air-conditioning plants. In attempting to monitor the presence of such hazardous particles, particle shape is a parameter that, taken with size, offers significant potential for particle identification and classification.

Optical-scattering techniques are widely used as a means of counting and sizing airborne particles on an individual basis and are embodied in a number of commercial instruments. However, in general these instruments do not attempt to assess particle shape

but rather attribute a spherical-volume-equivalent size to each measured particle, based on an empirical or theoretical calibration function. The accuracy and validity of such results has been the subject of some considerable study by researchers in the field, for example, Gebhart and Anselm,² Bottlinger and Umhauer,³ and Killinger and Zerull.⁴

Particle Shape Assessment

The authors have been investigating the extent to which the spatial intensity distribution, or scattering profile, of light scattered by individual airborne particles may be used to discriminate particles on the basis of shape as well as size, and to this end have developed instrumentation to capture transient scattering profiles from particles constrained within an airstream and delivered in single file through an illuminating laser beam (see below). The scattering profile of light scattered by any particle is determined primarily by its size (relative to the illuminating wavelength), its shape, and its orientation with respect to the incident illumination. Other factors including the dielectric structure of the particle and the polarization of the incident irradiation are also important. In attempting to derive shape and size information from unknown particles, therefore, the task is eased considerably if as many of the other variables as possible are controlled. In particular,

The authors are with the Engineering Research & Development Centre, University of Hertfordshire, Hatfield, Hertfordshire AL 10 9AB, UK.

Received 15 December 1993; revised manuscript received 22 March 1994.

0003-6935/94/307180-07\$06.00/0.

© 1994 Optical Society of America.

optimal control of particle orientation with respect to the incident illumination is a primary goal.

As an aid to developing optimized aerodynamic methods for orienting nonspherical particles within a sample air stream, studies have been carried out with aerosols containing particles of known and well-defined geometry and size, and scattering profiles from large numbers of individual particles have been recorded. To derive information relating to the particle orientation within the air stream from these scattering profiles, a simple theoretical treatment based on the Rayleigh-Gans formalism has been developed to model light-scattering behavior rapidly and routinely for each nonspherical particle species under test. The results of this exercise are described briefly in this paper.

Apparatus

The laser light-scattering instrument is described in detail elsewhere⁵ and is shown schematically in Fig. 1. The radiation source (not shown) is a linearly polarized 9-mW diode laser operating at a 670-nm wavelength and arranged with the beam axis perpendicular to the plane of the page, as shown in Fig. 1. Radiation from the laser is directed through a collimator, iris diaphragm, and cylindrical lens into the scattering chamber, where it strikes a 45° front silvered mirror (labeled 1), with the plane of polarization of the beam being perpendicular to the plane of incidence at the mirror. The radiation is focused to an approximately ellipsoidal cross section (3 mm width \times 120 μ m depth) at a point within the scattering chamber that is coincident with the transverse

flow of incoming sample air. The unscattered beam then passes on to a second 45° mirror and is subsequently absorbed within a baffle chamber.

Particle-laden air is drawn in through the scattering chamber in laminar flow at a rate of approximately 1.5 L min⁻¹ and is ensheathed by filtered air drawn in through lateral ports as shown in Fig. 1. The intersection of the airflow and the laser beam defines the scattering volume. Individual particles in the sample air transverse the laser beam and produce pulses of scattered light of $\sim 3 \mu$ s duration. Light scattered into angles between 28° and 141° to the beam direction and around the full 360° of azimuth is incident upon an ellipsoidal reflector whose primary focus is coincident with the scattering volume, in a fashion similar to that first used by Bartholdi *et al.*⁶ The reflected light is thus refocused to the secondary focus, where it passes through an iris diaphragm before being collimated by a lens assembly and directed onto the photocathode of an intensified charge-coupled device camera. The light falling on the photocathode is therefore a two-dimensional transform of the three-dimensional spatial intensity distribution falling onto the ellipsoidal reflector, and corresponds to approximately 82% of the total sphere of scattering about the particle. This image is the scattering profile.

To date, scattering profiles have been investigated for a range of particle shapes including spheres, sphere doublets, fibers, cubes, and flakes or platelets, and some of these are described by Kaye and coworkers.^{7,8} For the investigation of spherical particles, Mie theory (see, for example, Kerker⁹) was used to

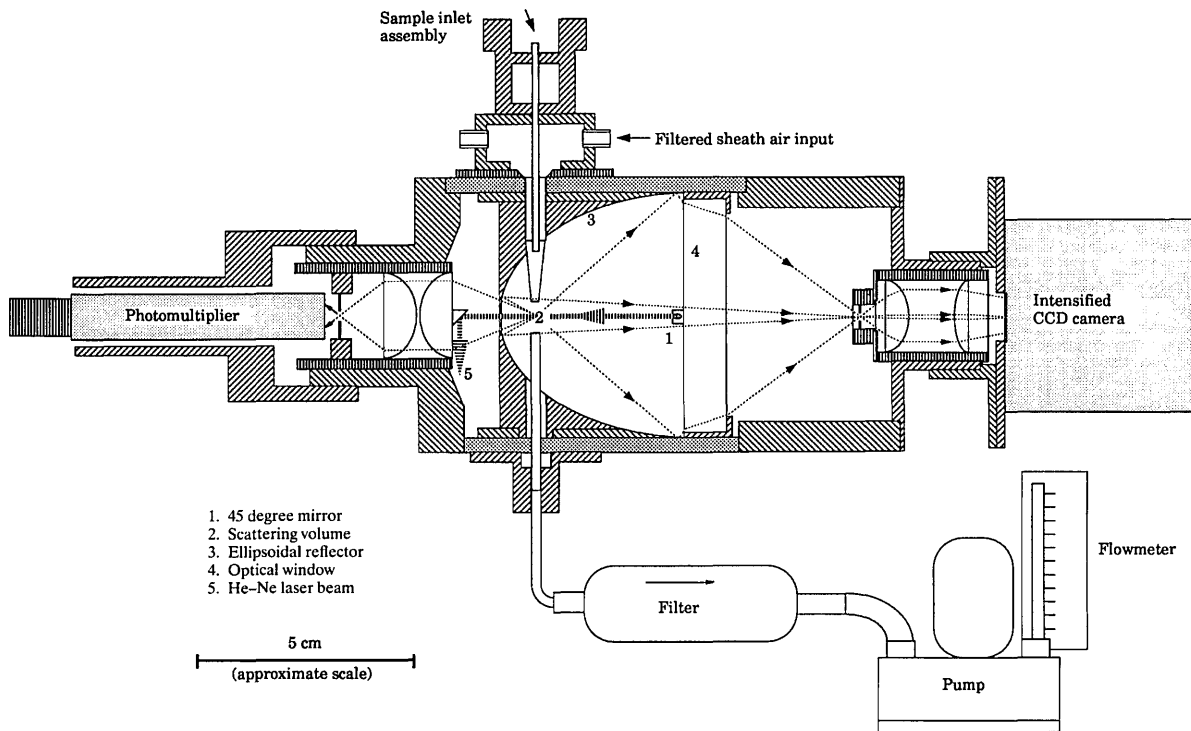


Fig. 1. Schematic diagram of optical-scattering chamber used to record spatial light-scattering data from individual particles carried within an airstream through a focused laser beam.

generate theoretical profiles with which experimental profiles could be compared. Kaye and coworkers also successfully used the Mie model to generate theoretical profiles corresponding to sphere doublets by considering the interference of two independently radiating spheres. In each of these cases close correlation between theory and experiment was observed.

However, for the particle orientation studies, we wished to model scattering from a variety of known nonspherical particle geometries. Foremost among these were silicon dioxide fibers produced by the process of silicon micromachining as first described by Hoover *et al.*¹⁰ These particles are characterized by an exceptionally high degree of dimensional accuracy and monodispersity, and the examples given in this paper relate to fiber particles that we have produced that have a square cross section ($1.5 \mu\text{m} \times 1.5 \mu\text{m}$), uniform length ($12 \mu\text{m}$), and a refractive index of $1.46 - i0.00$.⁷ Figure 2 shows a scanning electron micrograph of some of these particles.

Theoretical Model for Nonspherical Particle Scattering

Modeling the scattering behavior of these fibers and other nonspherical particles for various orientations relative to incident optical radiation could be achieved with established theoretical methods such as the method of moments described by Rao *et al.*¹¹ or the extended boundary condition method as described by Barber and Yeh.¹² However, because of their computational intensity and our limited computational resources (based on the ubiquitous IBM-PC), routine repetitive use of these methods for modeling large numbers of particle orientations was overly time consuming. A simplified treatment for the scattering behavior based on Rayleigh-Gans theory was therefore used, as described below. The Rayleigh-Gans theory assumes that the refractive index of the particle is close to 1 and that the phase shift of light passing through the particle is small, i.e.,

$$|m - 1| \ll 1, \quad kd|m - 1| \ll 1,$$

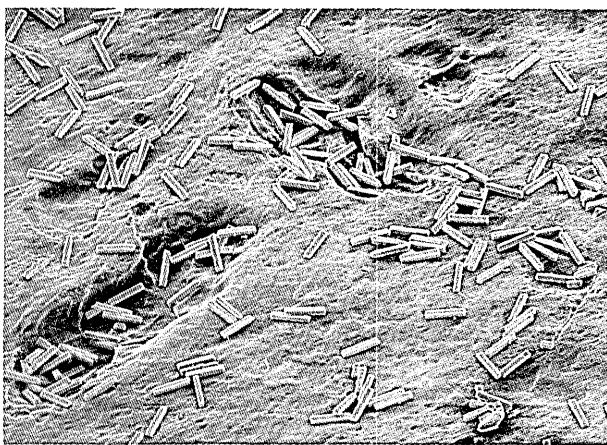


Fig. 2. Scanning electron micrograph of the silicon dioxide micromachined particles used as standard reference fibers in the study. The experimental scattering profiles shown in Figs. 3–5, below, were recorded from individual particles of this type.

where m is the refractive index, $k = 2\pi/\lambda$, and d is a relevant dimension of the particle.

The model represents the particle shape as a three-dimensional array of independent isotropic scattering points and determines the far-field interference effects when the array is illuminated from a specified direction. The resultant angular-intensity data are transformed as a computer-generated gray-scale image modified to take into account the geometric nonlinearity produced by the optical configuration of the instrument's scattering chamber. This facilitates direct comparison between theoretical and experimental scattering profiles.

Each theoretical profile comprises an image of 256×256 pixels. The model generates the profiles, one pixel at a time, by taking the pixel position expressed in polar coordinates around the center of the profile and using this information as an index to a lookup table. This table contains scattering directions that are expressed in the spherical coordinate angles θ and ϕ that are equivalent to the pixel positions, taking into account the nonlinearity produced by the optical system of the instrument. We generate the intensity for each pixel by considering the far-field interference resulting from a three-dimensional array of independent isotropic scattering points that define the particle shape. We determine the intensity by computing the interference that results from lines of scattering points along each of three orthogonal edges of the cuboid. For cuboidal particles, the interference for each edge can be expressed as the limit of a sum, and the total intensity is proportional to the product of these sums.

The relative phases of the scattering points are a function of their spatial positions in relation to the incident illumination. We find the relative phases between adjacent scattering points in three orthogonal directions parallel to orthogonal edges of the cuboid by first applying rotations α , β , and γ around the x , y , and z axes, respectively, to the points

$$[d \ 0 \ 0]^T, \quad [0 \ d \ 0]^T, \quad [0 \ 0 \ d]^T,$$

where d is the distance between scattering points along the edges of the cuboidal array. This permits the cuboidal array to have any orientation with respect to the illumination, which is incident along the z axis. The rotations are applied in the order β , α , γ and are given by the matrices

$$\begin{bmatrix} \cos \beta & 0 & -\sin \beta \\ 0 & 1 & 0 \\ \sin \beta & 0 & \cos \beta \end{bmatrix}, \quad \begin{bmatrix} 1 & 0 & 0 \\ 0 & \cos \alpha & -\sin \alpha \\ 0 & \sin \alpha & \cos \alpha \end{bmatrix},$$

$$\begin{bmatrix} \cos \gamma & -\sin \gamma & 0 \\ \sin \gamma & \cos \gamma & 0 \\ 0 & 0 & 1 \end{bmatrix},$$

respectively. The total phase difference for an adjacent pair of points along an edge of the cuboid is made

up of two components, one that is due to the orientation of the pair relative to the incident illumination and another that is due to the orientation of the pair relative to the scattering direction. The first component is given by the dot product of a unit vector \hat{k} in the illumination direction and a vector \mathbf{p} describing the orientation of the points. The second component is given by the dot product of a unit vector \hat{s} in the scattering direction and the vector \mathbf{p} . The total phase difference is then

$$2\pi(\mathbf{p} \cdot \hat{k} - \mathbf{p} \cdot \hat{s})/\lambda,$$

where λ is the wavelength of the incident illumination. The vector \hat{s} in Cartesian coordinates is

$$[\sin \theta \cos \phi \sin \theta \sin \phi \cos \theta]^T,$$

giving us a total phase difference δ_i for a pair of points,

$$\delta_i = 2\pi d[-x_i \sin \theta \cos \phi - y_i \sin \theta \sin \phi + z_i(1 - \cos \theta)]/\lambda,$$

where d is the distance between points and x_i, y_i and z_i are the coordinates of unit vectors along each edge of the rotated cuboid. Thus three phase differences δ_i are obtained for pairs of points parallel to the three orthogonal edges of the cuboid.

Because each scattering point has a constant phase relationship to adjacent points, the amplitude in any direction is given by

$$\begin{aligned} A &= |[1 + \exp(i\delta) + \exp(i2\delta) + \cdots + \exp(iN\delta)] \\ &= |[1 - \exp(iN\delta)]/[1 - \exp(i\delta)]| \\ &= \sin(N\delta/2)/\sin(\delta/2), \end{aligned}$$

where δ is the phase difference between adjacent scattering points parallel to an edge and N is the number of points. By writing the phase difference as

$$\hat{\delta} = \delta\lambda/2\pi d,$$

the amplitude as d becomes infinitesimally small is

$$A = S \sin(\pi S \hat{\delta}/\lambda)/(\pi S \hat{\delta}/\lambda),$$

where S is Nd , a side length of the cuboid. The total scattering amplitude is then given by

$$A_T = V \prod_{i=1}^3 \frac{\sin(\pi S_i \hat{\delta}_i/\lambda)}{\pi S_i \hat{\delta}_i/\lambda},$$

where V is the volume of the cuboid. The intensity of scattering is proportional to the square of this value. The constant of proportionality is chosen to produce profiles with intensities similar to those of the experimental profiles.

Results

Monodisperse aerosols of the specific particle types were generated with a method described elsewhere (Kaye *et al.*⁵) and then sampled with the light-scattering instrument. The scattering profiles generated by individual particle transits through the laser beam within the instrument scattering chamber are shown in Figs. 3–7, below.

Experimental Scattering Profiles

Each of the experimental profile images was captured in a period of 2 μ s during the particle transit through the laser beam and represents essentially a scattered photon distribution map, which is the result of several thousand photons scattered by the particle to the faceplate of the image intensifier. The innermost dark circle at the center of each image in Figs. 3–7, below, corresponds to scattering at 28° to the laser beam propagation axis, this axis being perpendicular to the plane of the paper. The outer circumference corresponds to scattering at 141° to the beam axis. These angular limits are defined by the geometry of the ellipsoidal mirror within the scattering chamber. The vertical dumbbell-shaped shadow [most visible in Fig. 5(a), below] is an artifact of the instrument that is caused by the sample airflow inlet and exit tubes; the centers of the two circular shadows thus represent 90° scattering directly above and below the particle.

Theoretical Scattering Profiles

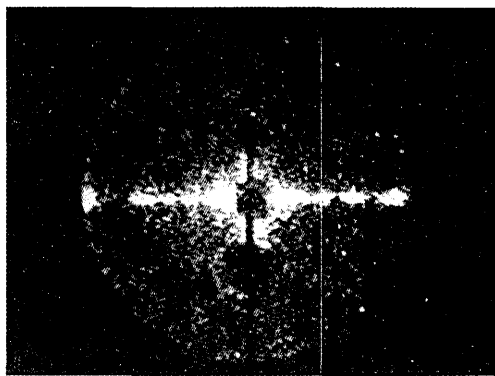
The theoretical profiles were generated with an IBM PC 386 type computer that used the mathematical treatment of a three-dimensional array of independent isotropic scattering points as described above. Processing time for each theoretical profile was approximately 61 s.

Profile Comparisons

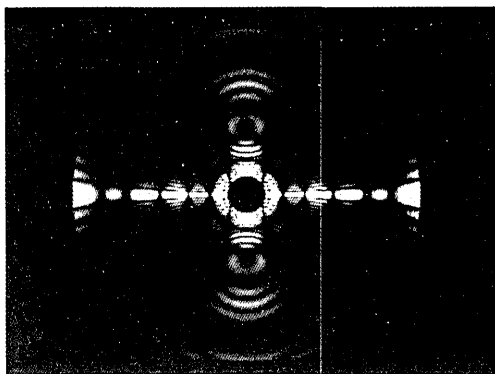
Figures 3(a), 4(a), and 5(a) show experimental scattering profiles generated by individual particles drawn from a monodisperse aerosol of silicon dioxide micromachined fibers. The cuboidal fiber had a 1.5 μ m \times 1.5 μ m cross section and a 12- μ m length. Approximately 2000 profiles from these fibers have been recorded, and they exhibited scattering behavior that was significantly dependent on the fiber orientation with respect to the laser beam, as would be expected.

Figure 3(a) corresponds to the classic case of a fiber that is aligned vertically, i.e., parallel to the axis of the sample airflow and perpendicular to the incident radiation, resulting in a horizontal linear scattering profile. Figure 3(b) shows the best-fit theoretical model for this scattering event, corresponding to a vertically oriented cuboid illuminated face on, as indicated in Fig. 3(c). The correlation between theory and experiment can be seen to be reasonably good.

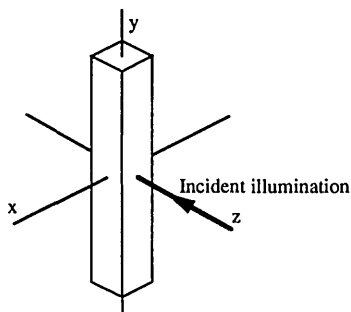
Figure 4(a) again exhibits predominantly horizontal scattering, implying vertical fiber orientation, but also exhibits spreading of the scattered radiation



(a)



(b)



(c)

Fig. 3. (a) Experimental scattering profile recorded from a single silicon dioxide fiber ($1.5 \mu\text{m} \times 1.5 \mu\text{m} \times 12 \mu\text{m}$). Each white dot corresponds to a single photon scattered to the image intensifier. The laser beam propagation axis is orthogonal to the plane of the page toward the center of the image. The inner dark circle circumference corresponds to scattering at 28° to the beam axis, and the outer circumference corresponds to scattering at 141° . The full 360° of azimuth is captured, and the image therefore corresponds to 83% of the total sphere of scattering about the particle. (b) Corresponding best-fit theoretical profile resulting from a fiber model illuminated as indicated in (c). (c) Schematic diagram showing the orientation of the theoretical fiber model with respect to the direction of incident illumination (indicated by the arrow). In this case the fiber has a face toward the illumination.

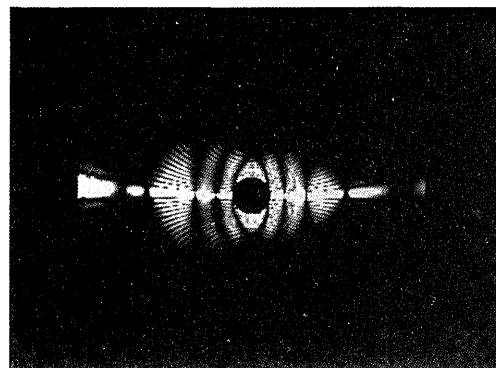
above and below this horizontal plane. The cause of this spreading was originally unclear, but in further theoretical modeling it was found that rotating the fiber model about its long axis produced a very similar effect, and Fig. 4(b) corresponds to such a rotation of magnitude 40° . The spreading may therefore be

attributed to the edge-on illumination of the fiber, as indicated in Fig. 4(c). (The theoretical best-fit data also include the effect of a 1° tilt of the fiber with respect to the vertical.)

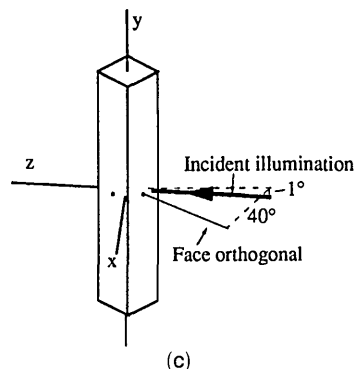
Figure 5(a) shows an experimental profile generated by a fiber misoriented from vertical, resulting in the scattering profile's adopting a conic-section form as predicted by Mie theory for infinite inclined cylinders (Bohren and Huffman¹³). Figure 5(b) shows the best-fit theoretical profile corresponding to a cuboidal



(a)

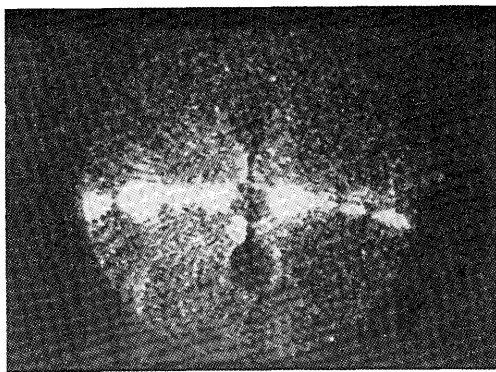


(b)

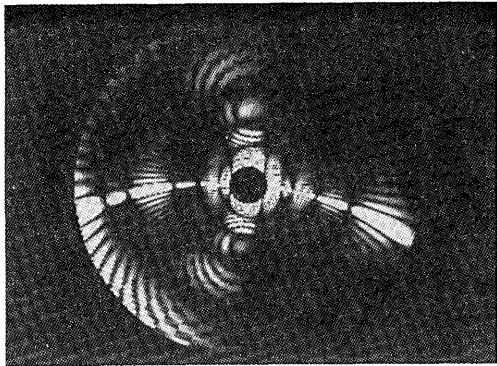


(c)

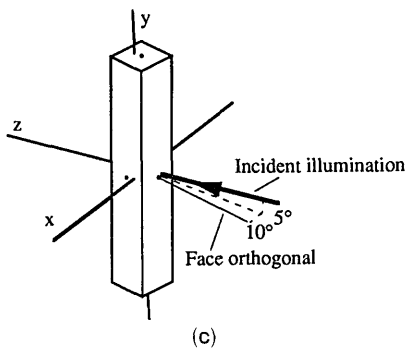
Fig. 4. (a) Experimental scattering profile from a silicon dioxide fiber identical in form to that which produced the data in Fig. 3(a). The image-acquisition time was $2 \mu\text{s}$. Here the spreading of the radiation in the vertical plane is related to edge-on illumination of the particle, as indicated in (c). (b) Corresponding best-fit theoretical profile resulting from a fiber model illuminated as indicated in (c). (c) schematic diagram showing the orientation of the theoretical fiber model with respect to the direction of incident illumination (indicated by the arrow). In this case the fiber is almost edge-on to the illumination.



(a)



(b)



(c)

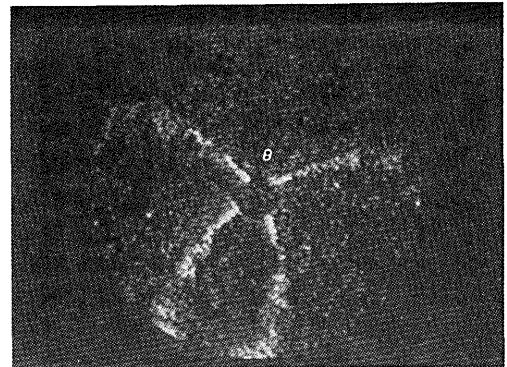
Fig. 5. (a) Experimental scattering profile from a silicon dioxide fiber identical in form to that which produced the data in Fig. 3(a). The scattering profile exhibits vertical spreading. The image-acquisition time was $2 \mu\text{s}$. (b) Corresponding best-fit profile resulting from a theoretical fiber model. (c) Schematic diagram showing the orientation of the theoretical fiber model with respect to the direction of incident illumination (indicated by the arrow). In this case the fiber is rotated 10° about its long axis. The 5° tilt from the vertical accounts for the main bar of scattering adopting a conic-section form.

array, as defined above, tilted 5° toward the incident beam and rotated through 10° about the long axis with respect to the incident beam [see Fig 5(c)]. Most of the features present in the experimental profile can be seen to be predicted by this theoretical model.

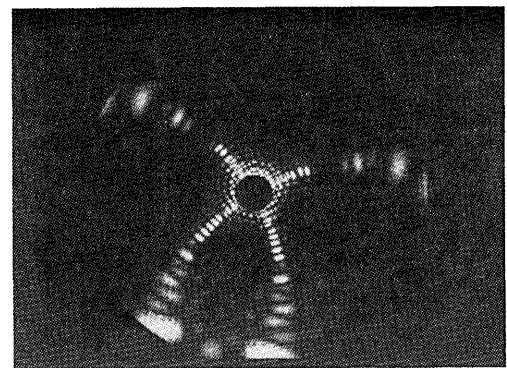
Figure 6(a) shows the experimental scattering profile generated by a single cubic salt crystal. The corresponding best-fit theoretical profile, Fig. 6(b), is that of a cube with $5\text{-}\mu\text{m}$ sides. As shown in Fig. 6(c), the direction of illumination was such that the

beam axis made an angle of 10.9° to the cube face in the horizontal plane and 6.3° in the vertical plane. Additionally, the cube was rotated 15° about the laser beam axis.

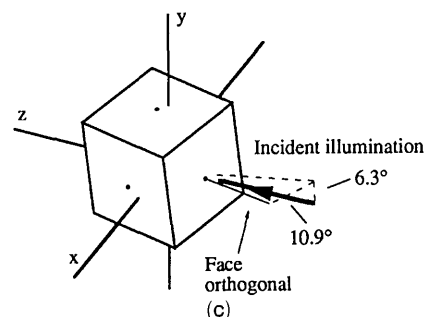
Figure 7(a) shows a scattering profile that was generated by a single particle from an aerosol of copper flakes. These irregularly shaped flakes were approximately $0.1 \mu\text{m}$ thick and typically $2\text{--}5 \mu\text{m}$ in their largest dimension. Figure 7(b) shows a theoretical profile corresponding to a square flake with a thickness of $0.1 \mu\text{m}$ and $3\text{-}\mu\text{m}$ sides. Because the exact form of the particle that generated the experimental profile was not known, the correlation between theoretical and experimental data is not as close as with the micromachined fibers. Neverthe-



(a)

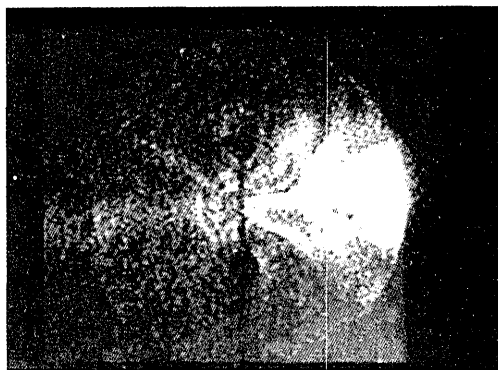


(b)

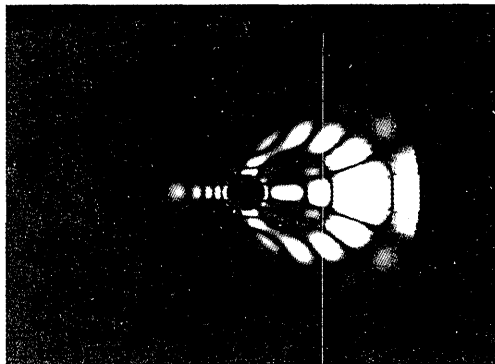


(c)

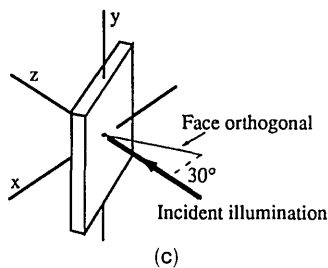
Fig. 6. (a) Experimental scattering profile from a single crystal drawn from an aerosol of salt crystals. The image-acquisition time was $2 \mu\text{s}$. (b) Best-fit theoretical profile corresponding to a cube with $5\text{-}\mu\text{m}$ sides. (c) Diagram showing the incident illumination direction in relation to the cubic array. A 15° rotation of the cube around the illumination direction was also applied to produce the profile in (b).



(a)



(b)



(c)

Fig. 7. (a) Experimental scattering profile from a single copper flake drawn from an aerosol. The image-acquisition time was 2 μ s. (b) Theoretical profile corresponding to a cuboid with 3- μ m sides and a thickness of 0.1 μ m. (c) Diagram showing the incident illumination direction (indicated by the arrow) in relation to the array of point scatterers used as the model in (b).

less, as can be seen in Fig. 7, the model does produce the main characteristics observed in the experimental profiles from these flakes.

Discussion

The results of these experimental and theoretical modeling exercises are now being used to aid in the design of inlet nozzles that not only deliver the airborne particles in single file through the laser beam scattering volume but also exhibit aerodynamic focusing properties to align nonspherical particles optimally with respect to the axis of the airflow. Controlling particle orientation during particle illumination by the laser makes the subsequent analysis of the scattering profiles considerably easier. In any future instruments that can be used in the field for real-time airborne particle monitoring that are based

on this technology, the limiting factor governing particle throughput will be the time for interpretation of the scattered light distribution, and however any reduction in the inherent complexity of the task is achieved, it will be beneficial.

The Rayleigh-Gans theory assumes that the refractive index of the particle is close to unity and that the phase shift of light that passes through the particle is small. Despite the fact that neither of these criteria is strictly met in the cases described in this paper, the theoretical model that is used allows us to interpret the main features of the experimental scattering correctly and to achieve this with comparative rapidity.

This work has been supported by a grant under the U.K. Science and Engineering Research Council/Ministry of Defence Joint Scheme.

References

1. J. G. Firth, "Future trends," in *Proceedings of the International Symposium—Clean Air at Work*, R. H. Brown, M. Curtis, K. J. Saunders, and S. Vandendriessche, eds. (Royal Society of Chemistry, London, 1992), pp. 469–473.
2. J. Gebhart and A. Anselm, "Effect of particle shape on the response of single particle optical counters," in *Proceedings of the International Symposium on Optical Particle Sizing, Theory and Practice* (Plenum, New York, 1988), pp. 393–409.
3. M. Bottlinger and H. Umhauer, "Scattered light particle-size counting analysis—influence of shape and structure," in *Proceedings of the International Symposium on Optical Particle Sizing, Theory and Practice* (Plenum, New York, 1988), pp. 363–369.
4. R. T. Killinger and R. H. Zerull, "Effects of shape and orientation to be considered for optical particle sizing," in *Proceedings of the International Symposium on Optical Particle Sizing, Theory and Practice* (Plenum, New York, 1988), pp. 419–429.
5. P. H. Kaye, E. Hirst, J. M. Clark, and F. Micheli, "Airborne particle shape and size classification from spatial light scattering profiles," *J. Aerosol Sci.* **23**, 597–611 (1992).
6. M. Bartholdi, G. C. Salzman, R. D. Heibert, and M. Kerker, "Differential light scattering photometer for rapid analysis of single particles in flow," *Appl. Opt.* **19**, 1573–1581 (1980).
7. P. H. Kaye, F. Micheli, M. C. Tracey, E. Hirst, and A. M. Gundlach, "The production of precision silicon micromachined nonspherical particles for aerosol studies," in *Proceedings of the 1992 European Aerosol Conference, Oxford* [*J. Aerosol Sci.* **23S1**, 201–204 (1992)].
8. P. H. Kaye, E. Hirst, and F. Micheli, "The characterisation of airborne particles by analysis of spatial light scattering profiles," in *Proceedings of the 1992 European Aerosol Conference, Oxford* [*J. Aerosol Sci.* **23S1**, 321–324 (1992)].
9. M. Kerker, *The Scattering of Light and Other Electromagnetic Radiation* (Academic, New York, 1969).
10. M. D. Hoover, S. A. Casalnuovo, P. J. Lipowicz, H. C. Yeh, R. W. Hanson, and A. J. Hurd, "Method for producing non-spherical monodisperse particles using integrated circuit fabrication techniques," *J. Aerosol Sci.* **21**, 569–575 (1990).
11. S. M. Rao, D. R. Wilton, and A. W. Glisson, "Electromagnetic scattering by surfaces of arbitrary shape," *IEEE Trans. Antennas Propag.* **AP-30**, 409–417 (1982).
12. P. Barber and C. Yeh, "Scattering of electromagnetic waves by arbitrary shaped dielectric bodies," *Appl. Opt.* **14**, 2864–2872 (1975).
13. C. F. Bohren and D. R. Huffman, *Absorption and Scattering of Light by Small Particles* (Wiley, New York, 1983), Chap. 8, p. 201.